Effect of furan π-spacer and triethylene oxide methyl ether substituents on performance of phenothiazine sensitizers in dye-sensitized solar cells†

Audun Formo Buene, [a] Nanna Boholm,[b] Anders Hagfeldt [c] and Bård Helge Hoff *[a]

Conjugated π-spacers are used to improve the light harvesting properties of sensitizers for dye-sensitized solar cells. In several recent works, furan has outperformed other popular π-spacers such as thiophene and phenyl. One of the best performing phenothiazine dyes in the literature has no π-spacer, and two polar triethylene oxide methyl ether (TEOME) chains. Herein we report the synthesis and evaluation of three novel sensitizers based on **EO3**, investigating the effect of introducing a furan linker and stepwise removal of the TEOME chains. The furan linker redshifted the onsets in the IPCE spectra by 50 nm and improved the PCE by up to 29% compared to **EO3**, despite lowering the V_{OC} by more than 60 mV. The best sensitizer of the study was **AFB-30**, with an average PCE of 5.86% (J_{SC} = 10.41 mA cm^{-2}, V_{OC} = 783 mV, FF = 0.73) under 1 sun AM 1.5G illumination.

Introduction

The introduction of dye-sensitized solar cells made quite a stir in 1991, when Michael Grätzel and Brian O'Regan published the remarkably efficient photoelectrochemical cell using light harvesting sensitizers anchored on mesoporous titania nanoparticles.[1] Since then, a number of great advancements have been made within the field of dye-sensitized solar cells (DSSCs). Although still popular, focus has largely moved from rare earth metal complex sensitizers to fully organic sensitizers.[2] Advantages such as higher extinction coefficients and a larger available toolbox of reliable organic reactions favour the organic sensitizers.[3]

Increasing the efficiency and stability is always a high priority in solar cell research. For the field of DSSCs, dye development strives to increase the light harvesting properties and the development of new semiconducting oxides and redox shuttles are improving the photovoltages of the devices.[4,5] Fully organic sensitizers are commonly based a donor–π–acceptor design, where the donor is an electron rich conjugated system such as triarylamine,[6] coumarins,[7,8] carbazole[9,10] or phenothiazine[11] among many others. The acceptor is electron deficient, often also acting as the anchoring group, resulting in a push–pull system which is transferring charge upon excitation. Because the photon flux in the solar spectrum is finite, increasing the absorption of the sensitizers is crucial in improving the photocurrents. A common design strategy to accomplish this is the introduction of π-spacers.[12] A range of spacers have been reported in the dye literature, ranging from the very simple, such as a single double bond,[13] various aromatic and heteroaromatic spacers,[14–16] to the more complex electron withdrawing units such as diketopyrrolo-pyrrole[17] or benzothiadiazole.[18]

Much effort has also been devoted to developing solid-state DSSCs,[19] and one of the most recent advancements is the discovery of the so-called 'Zombie cells' improving on the already efficient cells based on solid hole conducting materials such as spiro-OMeTAD.[20] Another direction for the DSSC field is the development of aqueous electrolytes.[21] Water has a higher boiling point than most organic solvents commonly used in DSSC electrolytes and most salts are excellently soluble in it. There are a number of aqueous iodide electrolytes reported in the literature,[21,22] and fully organic redox couple aqueous electrolytes have also successfully been developed.[23] The first aqueous cobalt electrolyte was reported by Spiccia *et al.* in 2013.[24] Later, cobalt complexes have been reengineered for increased water solubility avoiding the use of surfactants, producing very efficient aqueous DSSCs with 5.5% PCE.[25]

Despite the alluring advantages of aqueous electrolytes, the best power conversion efficiency of an aqueous DSSC reported

[a] *Department of Chemistry, Norwegian University of Science and Technology, Høgskoleringen 5, NO-7491 Trondheim, Norway. E-mail: bard.h.hoff@ntnu.no; Tel: +47 73593973*
[b] *Department of Chemistry, Aarhus University, DK-8000 Aarhus, Denmark*
[c] *Laboratory of Photomolecular Science, Institute of Chemical Sciences and Engineering, École Polytechnique Fédérale de Lausanne (EPFL), Chemin des Alambics, Station 6, CH-1015 Lausanne, Switzerland*

† Electronic supplementary information (ESI) available. See DOI: 10.1039/c9nj01720h

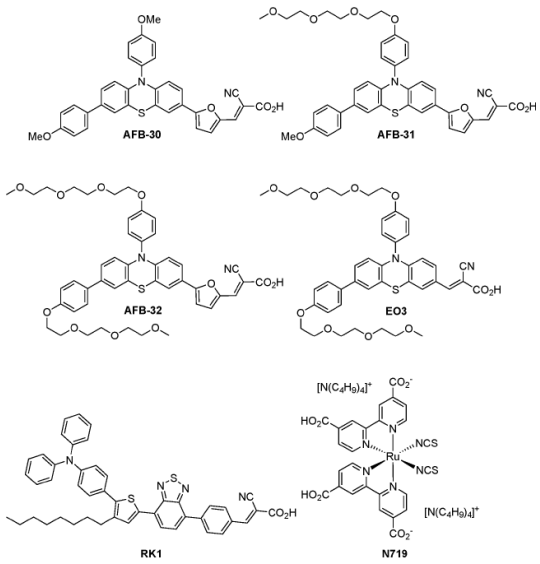

Fig. 1 Structures of sensitizers **AFB-30** to **32**, **EO3**, **RK1** and **N719**.

to date is a modest 5.97%, achieved by Lin and coworkers with the phenothiazine sensitizer **EO3**.[26] This sensitizer incorporates two hydrophilic TEOME chains, which increases the wetting of the TiO_2, chelates Li^+ ions, while also repressing sensitizer aggregation.[27–29] A remarkable efficiency of 9.98% PCE under 1 sun AM 1.5G illumination for **EO3** with an organic solvent-based electrolyte was also achieved, despite the very limited absorption onset of 551 nm.[26]

This study is focusing on improving the photophysical properties of **EO3** by introducing a π-spacer between the phenothiazine donor and the cyanoacrylic acid anchoring group. In a few recent publications, furan has been reported to outperform thiophene as a π-spacer.[12,30–32] Thus, we chose furan for extending the conjugation of **EO3**. We also wanted to investigate the effect of the TEOME chains, so in addition to **EO3**, three furan π-spacer dyes with zero, one and two TEOM-groups were synthesized, shown in Fig. 1.

Results and discussion

Synthesis

The synthesis of the literature dye **EO3** followed a synthetic route much the same as the one reported by Lin and coworkers.[26] An overview of the total reaction sequence is found in Scheme 1. All synthesis details can be found in the ESI.†

Compound **5** was prepared through a Buchwald–Hartwig cross coupling in over 10 g scale. Despite being a highly reliable reaction, the purification and removal of palladium are the challenges in this step. Further, a Vilsmeyer–Haack formylation on **5** gave compound **8** in 63% yield, and brominations with *N*-bromosuccinimide (NBS) gave compound **9** in 70% yield. In the penultimate step, a Suzuki coupling was employed to

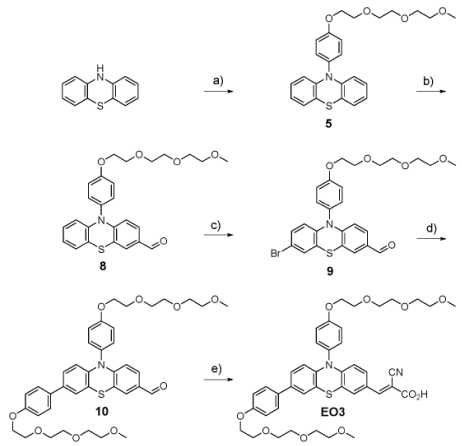

Scheme 1 Synthesis of **EO3**. (a) **2**, $Pd_2(dba)_3$, P(cy)$_3$, NaO*t*Bu, 120 °C, 66%, (b) DMF, $POCl_3$, 80 °C, 63%, (c) NBS, r.t., 70%, (d) **3**, $Pd(OAc)_2$, SPhos, K_2CO_3, 80 °C, 88%, (e) cyanoacetic acid, piperidine, 80 °C, 62%.

introduce the auxiliary donor in 80% yield using an aryl boronic ester prepared inhouse (**3**) before employing the Knoevenagel condensation for converting the aldehyde into the cyanoacrylic acid anchoring group present in all these sensitizers.

A route previously used by Iqbal and coworkers lay the foundations for the synthesis towards the AFB dyes, see Scheme 2.[33] A Buchwald coupling introduced the *N*-aryl substituents, while a dibromination with NBS separates this route from the previous method used for **EO3**. The brominations are efficient reactions and the products were obtained as convenient solid materials. Further, two sequential Suzuki cross couplings are performed. The first introduces the auxiliary donors in a non-selective manner also leading to the formation of the dicoupled byproducts, lowering the yields considerably. The second Suzuki coupling introduces the furan π-bridge from 5-formyl-2-furanylboronic acid, while the Knoevenagel condensation is used for the anchor group installation.

The melting points of the two dyes with two TEOME chains (**EO3** and **AFB-32**) were observed around 125 °C, while no melting point was observed for **AFB-30** and **31**. This suggests the TEOME chains decrease the crystallinity of the sensitizers. Upon further heating, visible decompositions were observed at the following temperatures: 145 °C (**AFB-31**) < 150 °C (**AFB-32**) < 170 °C (**EO3**) < 264 °C (**AFB-30**). We assume the observed decomposition is a decarboxylation because of visible gas formation. The high decomposition temperature of **AFB-30** was intriguing, and we suspected this to have one of two possible explanations. Either the presence of TEOME chains lowers the thermal stability, or the first decarboxylation step was not detected in the manual melting point analyses of **AFB-30**. We suspected the latter to be the case, because the molecular landscape around the anchoring cyanoacrylic acid is identical for all the AFB dyes, thus similar decarboxylation behaviours were expected. In order to conclude, we performed thermogravimetric analyses on all four dyes under air to investigate the decomposition as a function of temperature, and the results are plotted in Fig. 2.

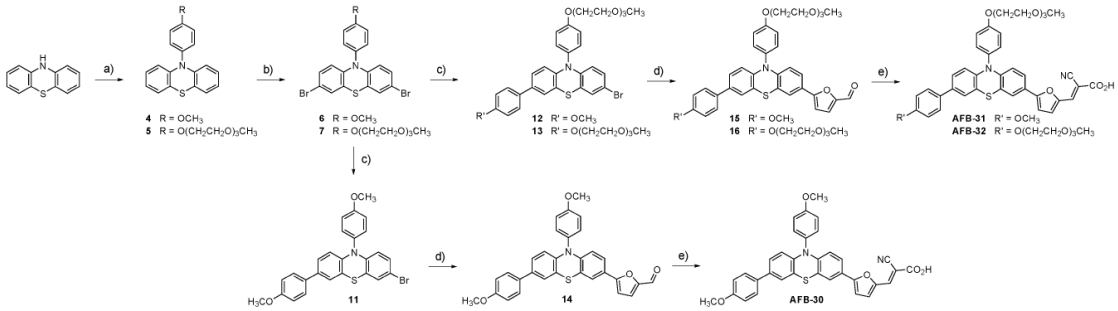

Scheme 2 Synthesis route to AFB dyes. (a) **2** or 4-bromoanisole, $Pd_2(dba)_3$, $P(cy)_3$, NaO*t*Bu, 120 °C, (b) NBS, r.t., (c) for prod. **11**/**12**: $Pd(PPh_3)_2$, K_2CO_3, 80 °C, **13**: $Pd(OAc)_2$, SPhos, K_2CO_3, 80 °C, (d) (5-formyl-2-furanyl)boronic acid, $Pd(OAc)_2$, SPhos, K_2CO_3, 80 °C, (e) cyanoacetic acid, piperidine, 80 °C.

A number of decomposition steps are observed for the four sensitizers in Fig. 2. The weight losses in the first steps are proportional in size to be attributed to decarboxylation processes. The decarboxylations are observed around 150 °C for all the AFB sensitizers while **EO3** does not decompose until 225 °C. This indicates the introduction of the furan π-spacer does affect the thermal stability negatively compared to **EO3**. Fortunately, despite the lowered thermal stability, under no part of the fabrication process or device operation will the sensitizers be subjected to temperatures in this range. However, it must be stressed that the chemical environment in devices cannot be compared to TGA analysis under air, so any device stability claims would have to be investigated by other means.

Photophysical properties

The solution and TiO_2 film UV/Vis absorption spectra of the three sensitizers and **EO3** are shown in Fig. 3, with the extracted data in Table 1. In solution, both hyper- and bathochromic shifts of the ICT band are observed upon the introduction of the furan π-spacer. In the region 350–400 nm a significant improvement in absorption can be seen for the AFB dyes as compared to **EO3** (Fig. 3a). This can only be attributed to the increase in conjugation from the furan unit. On TiO_2 films the differences are most prominent in the intensities of the ICT bands, and the relative extinction coefficients increased in the order **EO3** < **AFB-32** < **AFB-31** < **AFB-30**. The order mirrors the extinction coefficients from solution, but the differences are larger. This could be caused by minute variances in thickness of the TiO_2 films, but dye loading could also certainly play a role. The ICT peak position did not change when the dyes were anchored on TiO_2 compared to in solution, suggesting no aggregation issues with any of the dyes. However, a considerable broadening of the absorption was observed, shifting the absorption onset towards the red by about 50 nm.

From the emission spectra (Fig. S2, ESI†), a peak shift of 16–21 nm is observed when introducing the furan moiety.

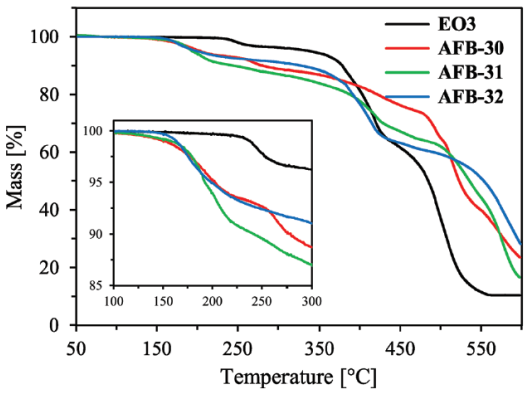

Fig. 2 Thermogravimetric curves for the four sensitizers measured under air atmosphere. Inset shows the decarboxylation region.

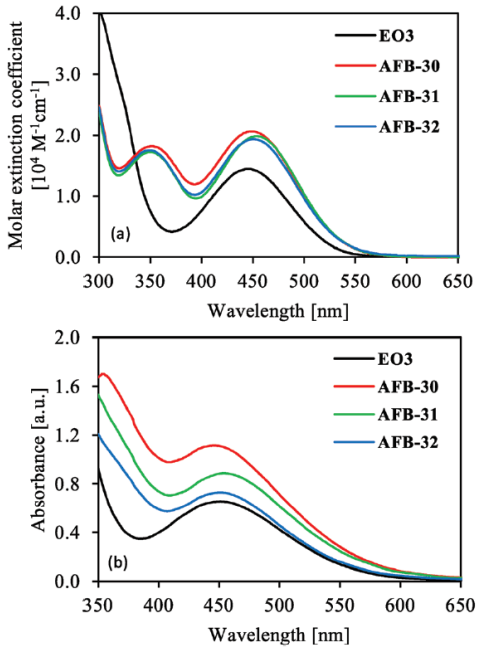

Fig. 3 UV/Vis absorption properties of sensitizers **AFB-30** to **32** compared to the literature dye **EO3**. (a) Measured in THF solution (0.02 mM), (b) measured on screen printed TiO_2 films (2.5 μm 18NR-T on TEC10 FTO glass).

Table 1 Photophysical properties of dyes **AFB-30** to **32** and **EO3**

Dye	λ_{abs}[a] (nm)	ε (M^{-1} cm^{-1})	Em.[b] (nm)	λ_{abs}[c] on TiO_2 (nm)	Rel. ε on TiO_2	$E_{0\text{-}0}$[d] (eV)	$E_{0\text{-}0}$[e] (eV)	E_{ox}[f] (V)	E_{LUMO}[g] (V)
EO3	446	14 448	584	451	1.00	2.38	2.36	1.07	−1.31
AFB-30	449	20 634	603	446	1.70	2.38	2.32	0.96	−1.42
AFB-31	454	19 844	605	454	1.36	2.39	2.32	0.93	−1.46
AFB-32	451	19 385	600	451	1.11	2.39	2.32	0.93	−1.46

[a] Maximum of most red-shifted peak. [b] Emission when ICT band is excited, in THF solution. [c] Maximum of most red-shifted peak on TiO_2 (2.5 μm, 18NR-T). [d] Calculated from the intersection of the absorption and normalized emission spectra in solution. [e] Calculated from the absorption onset in solution. [f] Measured *vs.* Fc^+/Fc on stained TiO_2 electrodes in acetonitrile with 0.1 M LiTFSI, converted to V *vs.* SHE by 0.624 V. Scan rate 20 mV s^{-1}. [g] Calculated from $E_{ox} - E_{0\text{-}0}$.

Despite the shifted peak positions, when the emission spectra are normalized to the absorption spectra, virtually identical optical bandgaps are obtained for all the four sensitizers from the absorption–emission intersection. We expected the increased conjugation from the furan moieties to lower the bandgaps. Optical bandgaps can alternatively be obtained by the absorption onset estimated from where the tangent to the ICT peak crosses the baseline. When using this method an optical bandgap of 2.36 eV is obtained for **EO3**, and 2.32 eV for all three AFB dyes, see Table 1.

Electrochemical properties

Cyclic voltammetry of the sensitizers adsorbed on TiO_2 was measured in acetonitrile with 0.1 M LiTFSI supporting electrolyte with a scan rate of 20 mV s^{-1}. The electrodes had no blocking layer, a 6 μm screen printed layer of 18 NR-T TiO_2 paste on FTO glass, no scattering layer and no CDCA in the staining solutions. The cyclic voltammograms can be found in the ESI† (Fig. S4). The $E_{1/2}$ value of Fc^+/Fc *vs.* Ag/AgCl was found at 0.2216 V. The subsequent measurements are given in Table 1 *vs.* SHE by the conversion constant of 624 mV.[34] We find the described method to be a highly efficient way of measuring the oxidation potentials of sensitizers, with the added benefit of the methodology being more closely related to actual device operating conditions. Reversible oxidation peaks were recorded for all the sensitizers. However, as the stability of the oxidized sensitizers usually is very limited, a fading of the signal is observed upon multiple cycles especially at low scan rates.

The oxidation potential of the literature dye **EO3** was found at 1.07 V *vs.* SHE, only 30 mV away from the reported value of 1.04 V *vs.* NHE in solution. Li and coworkers further developed **EO3** by closing one of the triethylene oxide methyl ether chains into a 12-crown-4 ether (**DCE1**).[35] The reported photophysical properties of **DCE1** are very similar to the values obtained for **EO3** in this work.

As the oxidation potential of **EO3** is 1.07 V *vs.* SHE, it is clear that the introduction of the furan π-spacer lifts the HOMO levels significantly, as presented visually in Fig. 4. The extracted oxidation potentials of **AFB-31** and **AFB-32** are indistinguishable by cyclic voltammetry at 0.93 V *vs.* SHE, while the value for **AFB-30** is slightly lower at 0.96 V *vs.* SHE. **AFB-30** is the only sensitizer without any TEOME chains, and the difference in oxidation potential could arise from the interactions of these moieties with the lithium cations present in the supporting electrolyte, marginally raising the oxidation potentials of **AFB-31** and **AFB-32**. For the I^-/I_3^- electrolyte, the HOMO and LUMO

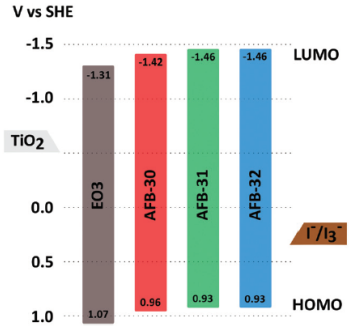

Fig. 4 Energy level diagram displaying the bandgap size and position of HOMO and LUMO of **EO3** and the AFB sensitizers.

positions are suitable for efficient electron injection and dye regeneration to take place.

Photovoltaic performance

The photovoltaic performance of the devices fabricated with the novel sensitizers, **EO3** and the references **N719** and **RK1**[36] was evaluated. Data from *J–V* sweeps under 1 sun AM 1.5G illumination and from incident photon-to-current conversion efficiency (IPCE) measurements are given in Table 2.

The photovoltaic measurements using the I^-/I_3^- electrolyte A6141[37] show that the introduction of the furan π-spacer increases the current, but at a considerable cost in the voltage, see Fig. 5. Similar behaviour in photovoltage has been observed previously in studies on phenothiazine dyes with and without π-spacers.[31,38] A direct comparison between **AFB-32** and **EO3**, only differing in the furan π-spacer, shows an increased performance by 16%. Among the AFB dyes, **AFB-30** is the most efficient at 5.86% PCE, comparable in performance to the literature dye **RK1** previously delivering over 10% PCE.[36] In the dark current measurements, no leaking could be observed from any of the devices, which confirms the recombination pathway from the TiO_2 to I_3^- is a slow process. From the IPCE measurements (Fig. 6) significant differences can be seen between **EO3** and the AFB dyes. The effect of the furan π-spacer can be seen clearly as increased power conversion in the region around 400 nm and an extension of the IPCE curves of about 60 nm towards longer wavelengths. A clear difference is observed in the absorption onsets between **EO3** and the AFB dyes in the IPCE spectra, suggesting the difference in optical bandgaps should be larger than those

Table 2 Photovoltaic performance under 1 sun AM 1.5G illumination of dyes **AFB-30**, **31** and **32**, compared to **EO3**, **RK1** and **N719**. Averages of three devices with corresponding standard deviations

Dye	Dye loading (10^{-7} mol cm^{-2})	IPCE J_{SC}[a] (mA cm^{-2})	J_{SC} (mA cm^{-2})	V_{OC} (mV)	FF	PCE[b] (%)
EO3	0.86	6.68	7.17 ± 0.19	829 ± 9.17	0.78 ± 0.01	4.53 ± 0.23
AFB-30	2.83	10.91	10.41 ± 0.34	783 ± 6.56	0.73 ± 0.01	5.86 ± 0.11
AFB-31	2.07	9.71	8.95 ± 0.24	764 ± 19.31	0.73 ± 0.01	4.91 ± 0.06
AFB-32	1.64	9.92	9.30 ± 0.26	763 ± 4.51	0.75 ± 0.02	5.25 ± 0.21
RK1	—	—	9.48 ± 0.26	778 ± 2.39	0.79 ± 0.01	5.81 ± 0.19
N719	—	—	12.82 ± 0.04	808 ± 4.40	0.74 ± 0.03	7.54 ± 0.32

[a] Obtained by integration of the IPCE spectrum over the 1 sun AM 1.5G spectrum. [b] Electrolyte composition 0.03 M I_2, 0.6 M 1-butyl-3-methylimidazolium iodide (BMII), 0.1 M guanidinium thiocyanate (GuSCN) and 0.5 M *tert*-butylpyridine in acetonitrile/valeronitrile (85 : 15, v/v).

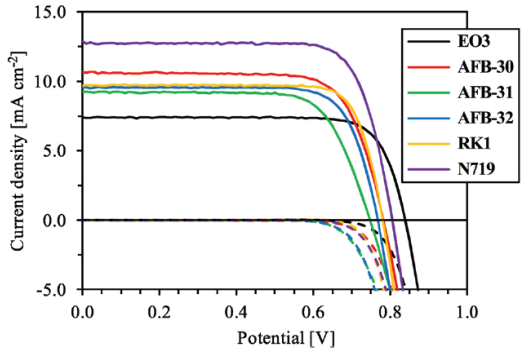

Fig. 5 *J–V* curves of the best device in each parallel. Corresponding dark current measurements included as dashed lines.

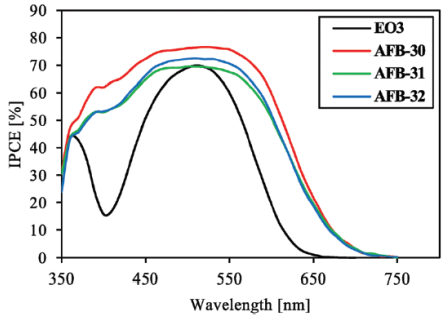

Fig. 6 IPCE spectra of dyes **EO3**, **AFB-30** to **32** with A6141 I^-/I_3^- electrolyte.

obtained from the UV/Vis-emission intersection method. The photocurrent response of the devices is redshifted compared to the photophysical measurements of the dyes. Part of this shift can be explained by the broadening of the absorption peak observed when the sensitizers were anchored on TiO_2, while the remaining difference must arise from interactions with the device electrolyte. Upon integration of the IPCE spectra, short-circuit current density estimates were obtained, which were within 8% of the J_{SC} values from the *J–V* sweeps under 1 sun illumination.

Dye loading measurements by desorption was performed in 40 mM tetrabutylammonium hydroxide in stabilized THF. For **AFB-30**, the dye loading is nearly identical to the reported value for the thiophene analogue **RD-SC**, recently reported by Liao *et al.*[39] Looking at dye **AFB-30** compared to **AFB-31** and **32**, it appears the presence of the TEOME chains reduces dye loading by up to 40%. While similar dye loading values for the two dyes with two TEOME chains (**EO3** and **AFB-32**) were expected, higher values were measured for **AFB-32**. A possible explanation could be the staining conditions favouring the dyes with furan π-spacer over **EO3**. The variance in dye loading in-part explain the efficiency differences. Likely, a more careful optimisation of CDCA concentration could increase the dye loading and efficiency of the devices based on TEOME containing dyes.

Inspired by the high performance of **EO3** in aqueous DSSC, we tested the four sensitizers in devices with the aqueous cobalt electrolyte $[Co(bpy\text{-}pz)_2]^{2+/3+}$ reported by Ellis *et al.*[25] The electrolyte composition was 0.13 M $[Co(bpy\text{-}pz)_2]Cl_2$, 0.06 M $[Co(bpy\text{-}pz)_2]Cl_3$ and 0.8 M 1-methylbenzimidazole (MBI) in deionized water. *J–V* curves and photovoltaic parameters are reported in the ESI† (Fig. S5 and Table S1). The average efficiencies were, in ascending order: **EO3** (0.17%) < **AFB-32** (0.18%) < **AFB-31** (0.40%) < **AFB-30** (0.57%). The open-circuit voltages were considerably lower than the ones previously reported for the $[Co(bpy\text{-}pz)_2]^{2+/3+}$ electrolyte, and **AFB-30** was again the most efficient sensitizer. The low efficiency could be a result of mismatched energy levels or unfavourable dye-electrolyte interactions, but the phenomenon has not been further investigated.

Attempting to further unnest the behaviour of these dyes, charge extraction and electron lifetime measurements were performed on the devices, see Fig. 7. The electron densities obtained from the charge extraction measurements (Fig. 7a) were comparable for all four dyes, with the highest values found for **AFB-32**. Also from these measurements, it is clear that dye **EO3** delivers a much higher V_{OC} than the AFB dyes. This could be the result of a conduction band shift, higher electron concentration or longer electron lifetimes. The charge extraction values (Q_{OC}) are direct measurements of the electron concentration in the TiO_2, and any conduction band shift may be found from the charge extraction measurements as a horizontal shift of one curve relative to another for the same Q_{OC} value. However, in order to determine the contribution of electron lifetime to the photovoltage, one has to correct for the conduction band shift and compare the electron lifetime measurements for the same charge densities, *i.e.* Q_{OC} values, as described previously[40] and shown in Fig. 7b.

Very little difference is found for the Q_{OC} values for the four sensitizers, but a large relative conduction band shift of

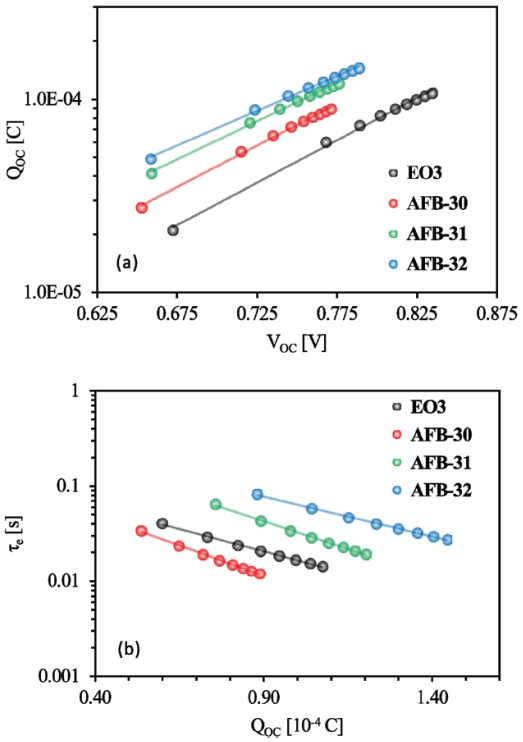

Fig. 7 (a) Charge extraction values measured at different light intensities, (b) electron lifetime measurements corrected for the observed conduction band shifts from (a) and then plotted *versus* the extracted charges at the same potentials. Devices fabricated with A6141 organic electrolyte.

approximately 80 mV is observed between **AFB-32** and **EO3**. From Fig. 7b we observe only small differences in electron lifetimes following the order of **AFB-30** < **EO3** < **AFB-31** < **AFB-32**. Considering the lower charge densities and electron lifetime values of **EO3** we would expect the actual difference in photovoltage to be lower than 80 mV. From the *J*–*V* sweeps, a shift of 66 mV is found, thus confirming the conduction band shift is the main contributor to the high V_{OC} for this dye.

Experimental

Synthesis

All details on the synthesis and characterization of the sensitizers in this work can be found in the ESI.†

Device fabrication

FTO glass (NSG10, Nippon Sheet Glass) was cut to size and cleaned with Deconex 21 (2 g L^{-1} in H_2O) in an ultrasonic bath for 45 minutes before being further cleaned in a UV/O_3 cleaner for 15 minutes. A TiO_2 blocking layer was deposited with hydrothermal deposition by immersion in an aqueous 40 mM $TiCl_4$ solution for 45 minutes at 70 °C then rinsed with deionized water and ethanol, repeated once. The mesoporous titania nanoparticle paste (18NR-T, GreatCellSolar) was screenprinted onto the FTO glass with a 54T mesh then dried at 125 °C for 5 minutes. Two layers of 18NR-T was deposited, followed by a scattering layer (WER2-O, GreatCellSolar) printed with the same screen. The total thickness of the active layer was measured to be 10 μm by profilometer. The titania electrodes were then sintered on a programmable hotplate with the ramping profile of 125, 250, 375, 450 and 500 °C for 5, 5, 5, 15 and 15 minutes with 5 minutes ramping time between each temperature step. $TiCl_4$ post treatment was performed on the electrodes by immersion in aqueous 40 mM $TiCl_4$ solution for 30 minutes at 70 °C, followed by rinsing with deionized water and ethanol. The photoanodes were completed by sintering on a hotplate at 500 °C for 45 minutes.

Counter electrodes were fashioned from TEC15 FTO glass, cut to size and holes for electrolyte filling were drilled with a diamond drill bit. The FTO slides were then cleaned with ultrasonication in Hellmanex solution, deionized water, ethanol and finally in acetone, each for 15 minutes. A solution of H_2PtCl_6 (10 mM in iso-propanol, 5 μL cm^{-2}) was dropcast on the individual electrodes and then they were fired at 400 °C for 15 minutes to leave only the catalytic layer of platinum.

Staining solutions had a concentration of 0.5 mM of dye and 5 mM of chenodeoxycholic acid. For the AFB dyes, a mixture of THF and acetonitrile (57 : 43, v/v) was used, while absolute ethanol was used for RK1 and a mixture of *tert*-butanol and acetonitrile (1 : 1, v/v) for N719. The electrodes were stained for 20 hours at room temperature before being rinsed in acetonitrile for 2 minutes, dried under air and sealed with the counter electrodes in a drybox using 25 μm thick Surlyn gaskets.

The A6141 electrolyte contained 0.03 M I_2, 0.6 M 1-butyl-3-methylimidazolium iodide (BMII), 0.1 M guanidinium thiocyanate (GuSCN) and 0.5 M *tert*-butylpyridine in acetonitrile/valeronitrile (85 : 15, v/v), and was injected by vacuum backfilling. The filling hole was sealed with Surlyn and a glass disk, and the protruding edges of the working and counter electrodes were covered in soldering tin from an ultrasonic soldering iron for lowered sheet resistance.

Device characterization

Current–voltage characteristics were measured under 1 sun AM 1.5G illumination from a solar simulator (Oriel, USA, 450 W) connected to a Keithley 2400. A black metal mask with an aperture of 0.16 cm^2 was used for all the measurements. Incident photon-to-current conversion efficiency measurements (IPCE) were measured on an Arkeo-Ariadne (Cicci Research s.r.l.) with a 300 W xenon lamp, from 350 to 750 nm. Electron lifetime and charge extraction measurements were performed with the Dyenamo Toolbox (Dyenamo, Sweden).

Conclusion

Three new sensitizers based on the efficient literature dye **EO3** were synthesized and evaluated with an I^-/I_3^- electrolyte. The photophysical and photovoltaic properties were improved and the best sensitizer, **AFB-30**, achieved an average PCE of 5.86%,

an improvement of 29% compared to **EO3**. The introduction of furan also shifted the HOMO levels towards more negative potentials, which could affect regeneration efficiency negatively when using cobalt or copper electrolytes with more positive E_{redox} than the I^-/I_3^- shuttle. Finally, the V_{OC} values obtained for the sensitizers were significantly reduced by the insertion of the furan moiety and a drop in V_{OC} of 46–66 mV compared to **EO3** was attributed to a relative conduction band shift. We also established through TGA measurements that the introduction of the furan π-spacer lowered the decomposition temperature compared to no π-spacer, but the decomposition temperatures are still sufficiently high for successful device fabrication and operation. These results indicate that there still is potential to improve even the best sensitizers. Lastly, we find that working on the phenothiazine scaffold is a careful balancing act, because you may improve the absorption properties, but at a considerable cost in photovoltage.

Conflicts of interest

There are no conflicts to declare.

Acknowledgements

Dr Nick Vlachopoulos is acknowledged for very helpful instructions on the cyclic voltammetry measurements, and Nikolai Helth Gaukås for the TGA analyses. The support from the Research Council of Norway to the Norwegian Micro- and Nano-Fabrication Facility, NorFab (project number 245963/F50) and the Norwegian NMR Platform (project number 226244/F50) is highly appreciated.

References

1 B. O'Regan and M. Grätzel, *Nature*, 1991, **353**, 737–740.
2 C.-P. Lee, R. Y.-Y. Lin, L.-Y. Lin, C.-T. Li, T.-C. Chu, S.-S. Sun, J. T. Lin and K.-C. Ho, *RSC Adv.*, 2015, **5**, 23810–23825.
3 Y. Hong, Z. Iqbal, X. Yin and D. Cao, *Tetrahedron*, 2014, **70**, 6296–6302.
4 A. Hagfeldt, G. Boschloo, L. Sun, L. Kloo and H. Pettersson, *Chem. Rev.*, 2010, **110**, 6595–6663.
5 Y. Saygili, M. Stojanovic, N. Flores-Díaz, S. M. Zakeeruddin, N. Vlachopoulos, M. Grätzel and A. Hagfeldt, *Inorganics*, 2019, **7**, 30.
6 A. Mahmood, *Sol. Energy*, 2016, **123**, 127–144.
7 K. D. Seo, H. M. Song, M. J. Lee, M. Pastore, C. Anselmi, F. De Angelis, M. K. Nazeeruddin, M. Grätzel and H. K. Kim, *Dyes Pigm.*, 2011, **90**, 304–310.
8 K. Hara, Z.-S. Wang, T. Sato, A. Furube, R. Katoh, H. Sugihara, Y. Dan-oh, C. Kasada, A. Shinpo and S. Suga, *J. Phys. Chem. B*, 2005, **109**, 15476–15482.
9 N. Koumura, Z.-S. Wang, M. Miyashita, Y. Uemura, H. Sekiguchi, Y. Cui, A. Mori, S. Mori and K. Hara, *J. Mater. Chem.*, 2009, **19**, 4829–4836.
10 K. Kakiage, Y. Aoyama, T. Yano, T. Otsuka, T. Kyomen, M. Unno and M. Hanaya, *Chem. Commun.*, 2014, **50**, 6379–6381.
11 R. M. El-Shishtawy, J.-D. Decoppet, F. A. M. Al-Zahrani, Y. Cao, S. B. Khan, M. S. Al-Ghamdi, B. G. Alhogbi, A. M. Asiri, S. M. Zakeeruddin and M. Grätzel, *New J. Chem.*, 2018, **42**, 9045–9050.
12 S. H. Kim, H. W. Kim, C. Sakong, J. Namgoong, S. W. Park, M. J. Ko, C. H. Lee, W. I. Lee and J. P. Kim, *Org. Lett.*, 2011, **13**, 5784–5787.
13 H. Tian, X. Yang, R. Chen, Y. Pan, L. Li, A. Hagfeldt and L. Sun, *Chem. Commun.*, 2007, 3741–3743.
14 N. V. Krishna, J. V. S. Krishna, S. P. Singh, L. Giribabu, L. Han, I. Bedja, R. K. Gupta and A. Islam, *J. Phys. Chem. C*, 2017, **121**, 6464–6477.
15 R. Li, X. Lv, D. Shi, D. Zhou, Y. Cheng, G. Zhang and P. Wang, *J. Phys. Chem. C*, 2009, **113**, 7469–7479.
16 B.-S. Chen, D.-Y. Chen, C.-L. Chen, C.-W. Hsu, H.-C. Hsu, K.-L. Wu, S.-H. Liu, P.-T. Chou and Y. Chi, *J. Mater. Chem.*, 2011, **21**, 1937–1945.
17 X. Sun, Y. Wang, X. Li, H. Agren, W. Zhu, H. Tian and Y. Xie, *Chem. Commun.*, 2014, **50**, 15609–15612.
18 S. Haid, M. Marszalek, A. Mishra, M. Wielopolski, J. Teuscher, J.-E. Moser, R. Humphry-Baker, S. M. Zakeeruddin, M. Grätzel and P. Bäuerle, *Adv. Funct. Mater.*, 2012, **22**, 1291–1302.
19 I. Benesperi, H. Michaels and M. Freitag, *J. Mater. Chem. C*, 2018, **6**, 11903–11942.
20 M. Freitag, Q. Daniel, M. Pazoki, K. Sveinbjörnsson, J. Zhang, L. Sun, A. Hagfeldt and G. Boschloo, *Energy Environ. Sci.*, 2015, **8**, 2634–2637.
21 F. Bella, C. Gerbaldi, C. Barolo and M. Grätzel, *Chem. Soc. Rev.*, 2015, **44**, 3431–3473.
22 F. Bella, S. Galliano, M. Falco, G. Viscardi, C. Barolo, M. Grätzel and C. Gerbaldi, *Chem. Sci.*, 2016, **7**, 4880–4890.
23 H. Tian, E. Gabrielsson, P. W. Lohse, N. Vlachopoulos, L. Kloo, A. Hagfeldt and L. Sun, *Energy Environ. Sci.*, 2012, **5**, 9752–9755.
24 W. Xiang, F. Huang, Y.-B. Cheng, U. Bach and L. Spiccia, *Energy Environ. Sci.*, 2013, **6**, 121–127.
25 H. Ellis, R. Jiang, S. Ye, A. Hagfeldt and G. Boschloo, *Phys. Chem. Chem. Phys.*, 2016, **18**, 8419–8427.
26 R. Y.-Y. Lin, F.-L. Wu, C.-T. Li, P.-Y. Chen, K.-C. Ho and J. T. Lin, *ChemSusChem*, 2015, **8**, 2503–2513.
27 J.-H. Yum, S.-J. Moon, C. S. Karthikeyan, H. Wietasch, M. Thelakkat, S. M. Zakeeruddin, M. K. Nazeeruddin and M. Grätzel, *Nano Energy*, 2012, **1**, 6–12.
28 S. Panagiotakis, E. Giannoudis, A. Charisiadis, R. Paravatou, M.-E. Lazaridi, M. Kandyli, K. Ladomenou, P. A. Angaridis, H. C. Bertrand, G. D. Sharma and A. G. Coutsolelos, *Eur. J. Inorg. Chem.*, 2018, 2369–2379.
29 D. Kuang, C. Klein, H. J. Snaith, J.-E. Moser, R. Humphry-Baker, P. Comte, S. M. Zakeeruddin and M. Grätzel, *Nano Lett.*, 2006, **6**, 769–773.
30 Z. Wan, C. Jia, Y. Duan, L. Zhou, Y. Lin and Y. Shi, *J. Mater. Chem.*, 2012, **22**, 25140–25147.
31 A. F. Buene, N. Uggerud, S. P. Economopoulos, O. R. Gautun and B. H. Hoff, *Dyes Pigm.*, 2018, **151**, 263–271.
32 M. Cariello, S. M. Abdalhadi, P. Yadav, J.-D. Decoppet, S. M. Zakeeruddin, M. Grätzel, A. Hagfeldt and G. Cooke, *Dalton Trans.*, 2018, **47**, 6549–6556.

33 Z. Iqbal, W.-Q. Wu, Z.-S. Huang, L. Wang, D.-B. Kuang, H. Meier and D. Cao, *Dyes Pigm.*, 2016, **124**, 63–71.
34 V. V. Pavlishchuk and A. W. Addison, *Inorg. Chim. Acta*, 2000, **298**, 97–102.
35 C.-T. Li, F.-L. Wu, C.-J. Liang, K.-C. Ho and J. T. Lin, *J. Mater. Chem. A*, 2017, **5**, 7586–7594.
36 D. Joly, L. Pellejà, S. Narbey, F. Oswald, J. Chiron, J. N. Clifford, E. Palomares and R. Demadrille, *Sci. Rep.*, 2014, **4**, 4033.
37 M. K. Nazeeruddin, F. De Angelis, S. Fantacci, A. Selloni, G. Viscardi, P. Liska, S. Ito, B. Takeru and M. Grätzel, *J. Am. Chem. Soc.*, 2005, **127**, 16835–16847.
38 H. Tian, X. Yang, J. Cong, R. Chen, J. Liu, Y. Hao, A. Hagfeldt and L. Sun, *Chem. Commun.*, 2009, 6288–6290.
39 X. Liao, H. Zhang, J. Huang, G. Wu, X. Yin and Y. Hong, *Dyes Pigm.*, 2018, **158**, 240–248.
40 A. F. Buene, E. E. Ose, A. G. Zakariassen, A. Hagfeldt and B. H. Hoff, *J. Mater. Chem. A*, 2019, **7**, 7581–7590.